Flexible relaxor materials: Ba2PrxNd1–xFeNb4O15 tetragonal tungsten bronze solid solution

Elias Castel, Michaël Josse, Dominique Michau, Mario Maglione

Flexible relaxor materials: $Ba_2Pr_xNd_{1-x}FeNb_4O_{15}$ Tetragonal Tungsten Bronze solid solution

Elias Castel, Michaël Josse, Dominique Michau, and Mario Maglione*

ICMCB-CNRS, 87, Avenue du Docteur Schweitzer, 33608 Pessac cedex, France

* To whom correspondence should be addressed: maglione@icmcb-bordeaux.cnrs.fr

Abstract

Relaxors are very interesting materials but they are most of the time restricted to perovskite materials and thus their flexibility is limited. We have previously shown that tetragonal tungsten bronze (TTB) niobates $Ba_2PrFeNb_4O_{15}$ was a relaxor below 170K and that $Ba_2NdFeNb_4O_{15}$ displays a ferroelectric behavior with a T_C =323K. On scanning the whole solid solution $Ba_2Pr_xNd_{1-x}FeNb_4O_{15}$ (x= 0, 0.2, 0.4, 0.5, 0.6, 0.8, 1), we demonstrate here a continuous cross over between these end member behaviors with a coexistence of ferroelectricity and relaxor in the intermediate range. This tuneability is ascribed to the peculiar structure of the TTB networks which is more open than the classical perovskites. This allows for the coexistence of long range and short range orders and thus opens the range of relaxor materials.

Because of their useful dielectric and piezoelectric properties, relaxors are under deep investigations nowadays.[1, 2, 3] At present, most of relaxors belong to the perovskite family and a lot of these are containing lead ions. We already showed that lead-free perovskites are more flexible than lead-containing ones because a continuous cross over from ferroelectric to

relaxor is observed in many solid solutions.[4, 5] A possible coexistence of ferroelectric and relaxor states in the same material would be a step further in favor of lead free materials. In the case of close packed perovskite structure such a coexistence has already been reported in Sodium Bismuth Titanate based compositions $Na_{0.5}Bi_{0.5}TiO_3$[6, 7] or in the $BaTiO_3$ family like $Ba_{0.9}Bi_{0.067}(Ti_{1-x}Zr_x)O_3$ ceramics.[8] The origin of such a coexistence in these Bismuth containing materials is however still a matter of debate.

We show here that a more opened crystalline network like the so-called Tetragonal Tungsten Bronze structure is able to trigger such a coexistence in a much obvious way. As shown in of figure 1, the TTB structure is based on interconnected octahedra leaving three different channels of 3-fold, 4-fold and 5-fold pseudo-symmetry. Numerous cations can be hosted within such channels thus opening a wide range of interesting compositions.[9, 10] Starting from $Ba_{2,5}Nb_5O_{15}$ where only the 4 and 5-fold channels are occupied by Barium, it was already shown that the 4-fold channels may be filled by a lanthanide ion (Ln) provided that a related amount of Fe is substituted to Nb within the octaedra for sake of preserving the overall lattice neutrality. The resulting $Ba_2LnFeNb_4O_{15}$ have appealing properties, including composite multiferroic at room temperature.[11,12]

Here, we want to show that, when the rare earth cationic site is occupied by a mixture of Praseodymium (Pr) and Neodymium (Nd), a continuous solid solution is obtained which exhibits very interesting behaviors when scanning the composition from Nd to Pr. First, the high temperature ferroelectric transition which is a common feature of a lot of TTBs, just collapses without a significant shift of the transition temperature. In the same time, a low temperature relaxor state grows and ferroelectricity is totally suppressed in the Pr pure

compound. These features which are hardly observed in other ferroelectric materials like perovskites will be discussed in view of the specific structure of the TTB network.

Before describing the dielectric data, we summarize briefly all the processing, shaping and characterization that we undertook to ensure high quality and reproducible ceramics. These important steps will be described in more details elsewhere. After optimized synthesis and sintering, powder X-ray Diffraction evidenced a pure TTB phase for all compositions $Ba_2Nd_{1-x}Pr_xFeNb_4O_{15}$ from x = 0 to 1 with no spurious phase in the limit of 0.5% (figure 2). The symmetry for all powders was tetragonal P4/mbm at room temperature. The lattice parameters and unit volume of these TTB changed continuously following the Vegard's law which states that the lattice parameters of the solid solution is a linear combination of the end members one. On the figure 3, we show that the unit cell volume is linearly increasing when the composition changes from Nd to Pr. On the x axis of this Vegard law, we have reported the equivalent rare earth ionic volume instead of the Praseodymium content x. This is to show that the unit cell volume is directly proportional to the effective ionic size at the A site of the TTB structure.

X-Ray microprobe analysis confirmed that the amount of spurious phases is only marginal and that it is independent of the given composition x. These first observations confirm that all changes in the dielectric properties do not originate from uncontrolled segregation of phases. In addition, scanning electron microscopy showed that the shape and size distribution of grains in the final ceramics were similar all over the solid solution and the porosity was low. In particular we observed the mean grain size of all our ceramics stays constant to about 20±10 μm. The compactness of all the studied pellets was better than 92% as computed from density measurements.

Dielectric measurements were performed on ceramic disks (8 mm diameter, 1 mm thickness) after deposition of gold electrodes on the circular faces by cathodic sputtering. The real and imaginary relative permittivities ε'_r and ε''_r were determined under dry helium as a function of both temperature (77–420 K) and frequency (10^2 – 10^6 Hz) using Hewlett Packard 4194 impedance analyzer.

As shown on figure 4, three different behaviors are observed in dielectric experiments for $Ba_2Pr_xNd_{1-x}FeNb_4O_{15}$ samples,

- for x=0, we observe one sharp peak of ε'_r, at about T=320K with no frequency dispersion as expected for a ferroelectric transition. Let us emphasis that the temperature variation of ε'_r within the paraelectric state at T>320K is not following the classical Curie-Weiss law as observed in all TTBs.[15]

- for x=1, a strong frequency dispersion of ε'_r and ε''_r occurs whose features fit well with a relaxor transition.

- for 0<x<1, as exemplified in figure 4 for x=0.6, both the high temperature ferroelectric transition and the low temperature relaxor maximum coexist. We note that such a sequence paraelectric - ferroelectric - relaxor states is still a matter of debate in the literature.[4, 14, 15]

For all compositions, the high temperature increase of ε''_r signs the conductivity contribution to the dielectric parameters in this temperature range. To underline the stability of the intermediate state, we have plotted on figure 5 the qualitative evolution of the ferroelectric and relaxor temperature (taken at 1 MHz) as a function of x. This shows that, unlike perovskite materials, the Pr/Nd substitution in TTB does not change much the

ferroelectric as well as the relaxor temperature. Within this intermediate ferroelectric range, polarization hysteresis loops are recorded with saturated polarization below 1 μC/cm^2 which is consistent with what was reported for similar rare earth containing TTB[16] . The gradual suppression of ferroelectricity under introduction of Pr is clearly evidenced on figure 6 where the hysteresis loops are disappearing on going from the Nd pure phase to the Pr one.

However, not changing the temperature does not mean that the Pr substitution leaves the respective ferroelectric and relaxor states unaffected. As usual for relaxors, we fitted the low temperature dielectric dispersion using the Vogel-Fulcher equation $\omega = \omega_0 . \exp(\frac{E_A}{k_B (T - T_{VF})})$ [17,18,19].

As shown on table 1, both the activation energy E_A and the Vogel-Fulcher temperature T_{VF} shift continuously with the Pr content x. This is also supported by the dispersion which increases strongly in the same time. This changes in the detailed relaxor parameters means that the microscopic origin of the relaxor state depends on the Pr content. As shown on figure 5, this substitution also alters a lot the ferroelectric transition peak. Indeed, we have plotted (figure 7a) in a normalized way the dielectric permittivity for all investigated composition only for one frequency (f = 1MHz) for sake of clarity. We clearly see that the ferroelectric peak collapses at a fixed temperature while the relaxor state grows. In the intermediate range, the co-existence of both the ferroelectric and relaxor states stems from a linear superposition of the end member behavior as confirmed by the computed curves in figure 7b where we have used $\varepsilon'_r(x)=x\varepsilon'_r(1)+ (1-x)\varepsilon'_r(0)$. The agreement between figures 7a and 7b confirms that there are no extra contributions in the intermediate composition range at least for the position and shape of the dielectric peaks. This is rather unusual in ferroelectric materials and TTB are thus more flexible than standard closed pack structures like perovskites.

We next want to discuss why the ferroelectric peak collapses without a significant change of the transition temperature. Even, if the Curie-Weiss law is not valid for TTBs, we can use a very crude approximation to understand why the dielectric maximum decreases while its temperature of occurrence stays. Within a full order disorder model[20, 21], the Curie constant which fixes the maximum reached ε'_r is related to the density of dipoles in the high temperature paraelectric state. When those dipoles are originating from correlated chains, the Curie constant C is inversely proportional to the density N of correlated chains.[22, 23, 24] As a result, one can write and $\varepsilon'_r \propto \frac{C}{T - T_C}$ and $C \propto \frac{1}{N}$. If the density of chains decreases, C increases and the maximum reached ε'_r decreases and eventually disappears without affecting the transition temperature T_C. We thus can state that our samples containing only Nd (x=0) have a small density of long chains and a well defined maximum of ε'_r is recorded. On the other hand, the Pr containing samples include a high density N of small chains and thus the maximum of ε'_r collapses. We next need to find an origin for this cutting down of ferroelectric correlation chains when the amount of Pr increases. Such a model is out of the scope of the present letter but we can recall that, the suppression of ferroelectric correlation usually results from mass, volume or charge imbalance among substituted cations.[25, 26]

Without excluding them, we can state that the mass and volume change under Pr substitution are not the main driving force. Indeed, in such case, noticeable structural changes as well as strong shifts in the ferroelectric transition temperature are expected and these are not observed here. We thus can look for differences in the electronic states: Pr may carry at least two valencies (III and IV) while Nd has a fixed III state. As a consequence, for sake of neutrality, the valency of Fe which is sitting at the ferroelectric active site within the oxygen octahedron can also be balanced between III and II (or the valency of Niobium may change

from V to IV). However, preliminary Mossbauer analysis did not evidenced Fe^{2+} in the x=1 ceramics. Whatever the microscopic mechanism, the main outcome of this may be a change in the Nb-O correlation chains and so the polar units will be split and their density N increased. By the way, such decrease of ferroelectric correlation under increasing of the Pr content is also able to induce the relaxor low temperature state and effect that is seen on the figures 4 and 7a would be fully explained. This very simple model will need further investigations such as Raman scattering but we stress again on the main result that we reported here: the flexibility of the opened TTB network allows for a tuning of the ferroelectric to relaxor cross over on scanning the composition from Nd to Pr in $Ba_2Nd_{1-x}Pr_xFeNb_4O_{15}$.

Acknowledgements

The authors want to thanks E. Lebraud and S. Pechev for the collection of X-Ray diffraction data, and A. Fargues for polishing the samples

References

[1] W. Ma and L.E. Cross, Appl. Phys. Lett. **78**, 2920 (2001)

[2] A.A. Bokov and Z.-G. Ye, J. Mater. Sci. **41**, 31 (2006)

[3] D. Damjanovic, M. Budimir, M. Davis and N. Setter J. Mater. Sci. **41**, 65 (2006)

[4] A. Simon, J. Ravez and M. Maglione, J. Phys.: Cond. Matter **16**, 963 (2004)

[5] J. Ravez, C. Broustéra and A. Simon, J. Mater. Chem **9**, 1609 (1999)

[6] J. Kreisel, A. M. Glazer, P. Bouvier and G. Lucazeau, Phys. Rev. B **63**, 174106 (2001)

[7] J.R. Gomah-Pettry, S. Saïd, P. Marchet and J.P. Mercurio, J. Eur. Ceram. Soc. **24**, 1165 (2004)

[8] A. Simon, J. Ravez and M. Maglione, Sol. Sta. Sci. **7**, 925 (2005)

[9] A. Magneli, Arkiv. Kemi. **24**, 213 (1949)

[10] M. Pouchard, J.-P. Chaminade, A. Perron, J. Ravez and P. Hagenmuller, J. Sol. Sta. Chem. 14, 274 (1975)

[11] P.H. Fang and R.S. Roth, J. Appl. Phys. **31**, 143 (1960)

[12] E. Castel, M. Josse, F. Roulland, D. Michau, L. Raison and M. Maglione, J. Magn. Magn. Mater., **321-**11, 1773 (2009)

[13] C. Perrin, N. Menguy, O. Bidault, C. Y. Zahra, A.-M. Zahra, C. Caranoni, B. Hilczer and A.

Stepanov, J. Phys.: Cond. Matter **13**, 10231 (2001)

[14] G. A. Samara and L. A. Boatner, Phys. Rev. B **61**, 3889 (2000)

[15] M. Josse, O. Bidault, F. Roulland, E. Castel, A. Simon, D. Michau, R. Von der Mühll, O.

Nguyen and M. Maglione, Sol. Sta. Sci., **11**, 1118 (2009)

[16] I.W. Chen, J. Phys. Chem. Sol. **61**, 197 (2000)

[17] D. Viehland, S. J. Jang, L. E. Cross, and M. Wuttig, J. Appl. Phys. **68**, 2916 (1990)

[18] H. Vogel, Phys. Z. **22**, 645(1921)

[19] G. S. Fulcher, J. Am. Ceram. Soc. **8**, 339 (1925)

[20] F. Jona and G. Shirane, *Ferroelectric Crystals* (MacMillan, New York, 1962), pp. 152–253

[21] G. Burns and B.A. Scott, Phys. Rev. B 38, 597 (1988)

[22] R. Comes, M. Lambert and A. Guinier, Sol. Sta. Comm. **6**, 715 (1968)

[23] A. M. Quittet and M. Lambert, J. Phys. Col. **33**, C2-141 (1972)

[24] R. Yu and H. Krakauer, Phys. Rev. Lett. **74**, 4067 (1995)

[25] W. Cochran, Adv. Phys. **10**, 401 (1961)

[26] J.F. Scott, Phys. Rev. B **4**, 1360 (1970)

Figure captions

Figure 1: Crystal structure of $Ba_2LnFeNb_4O_{15}$ viewed along the c axis. The Ba and Ln cations occupy the 5-fold and 4-fold sites respectively while the ferroelectric active Nb cations site at the center of the oxygen octahedral.

Figure 2: XRD patterns for $Ba_2Pr_xNd_{1-x}FeNb_4O_{15}$ (x= 0, 0.2, 0.4, 0.5, 0.6, 0.8, and 1) ceramics. Arrows are drawn into the XRD patterns inset plotted in a semi logarithmic scale to emphasis the $LnNbO_4$ secondary phase which is independent on x.

Figure 3: The unit cell volume plotted versus the equivalent rare earth ionic volume $V_{Ln^{3+}}$.

Figure 4: Real (top frame) and imaginary permittivity (bottom frame) for x =0, 0.6 and 1. The operating frequency is scanned from 10^2 to 10^6 Hz from top to bottom. The high temperature increase of ε" stems from a conductivity contribution.

Figure 5: Qualitative phase diagram of $Ba_2Pr_xNd_{1-x}FeNb_4O_{15}$ evidencing coexistence between ferroelectricity and relaxor state in the intermediate composition range. Note that both the ferroelectric and relaxor temperatures are nearly independent on the composition.

Figure 6: Ferroelectric hysteresis loops at 280K, evolution of the polarization of the $Ba_2Pr_xNd_{1-x}FeNb_4O_{15}$ samples under 1.6±0.2kV/cm.

Figure 7: (a) Normalized dielectric data at 1MHz for the whole set of compositions $Ba_2Pr_xNd_{1-x}FeNb_4O_{15}$ $0<x<1$; in (b) the curves for the intermediate compositions ε(x,T) have been reconstructed by a linear superposition of the end members ε(0,T) and ε(1,T).

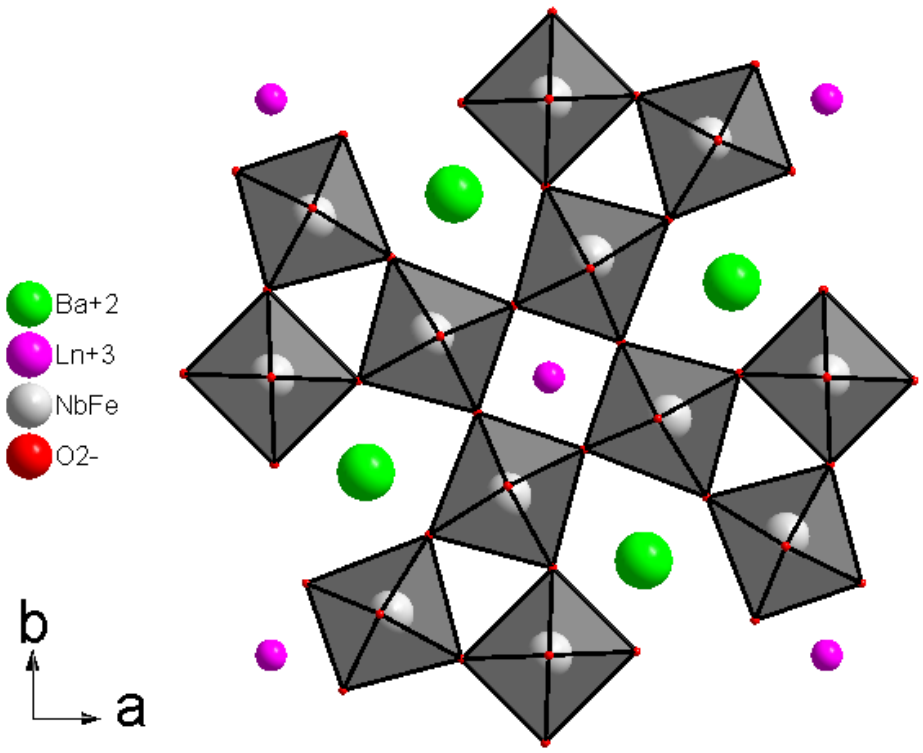

Figure 1

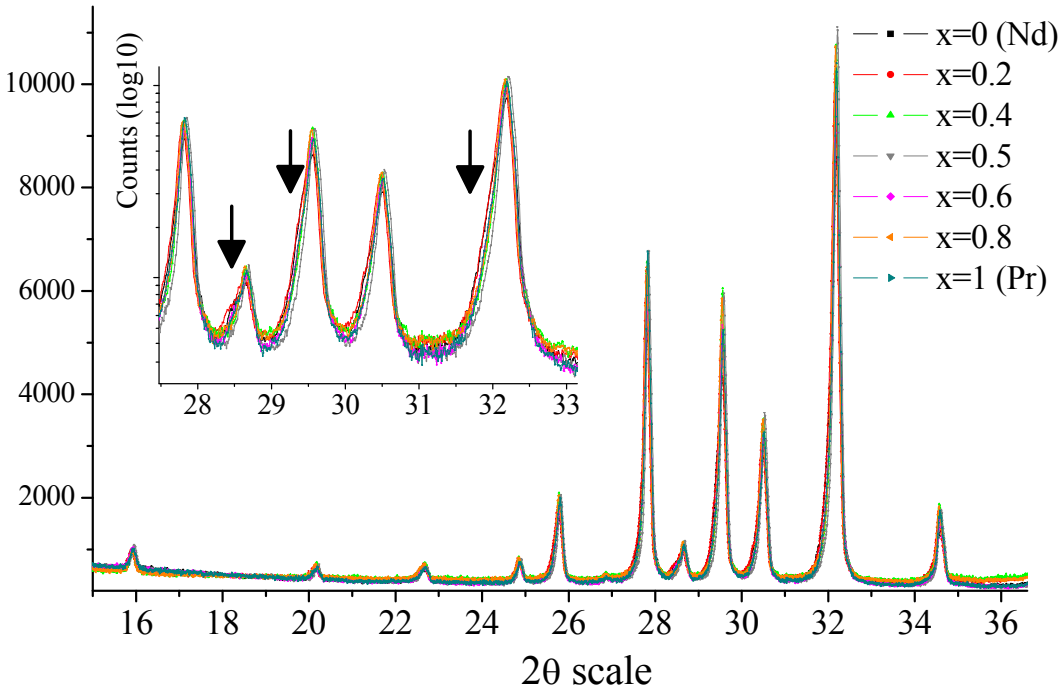
Counts (log10)
10000
8000
6000
4000
2000
28
29
30
31
32
33
x=0 (Nd)
x=0.2
x=0.4
x=0.5
x=0.6
x=0.8
x=1 (Pr)
16
18
20
22
24
26
28
30
32
34
36
2θ scale

Figure 2

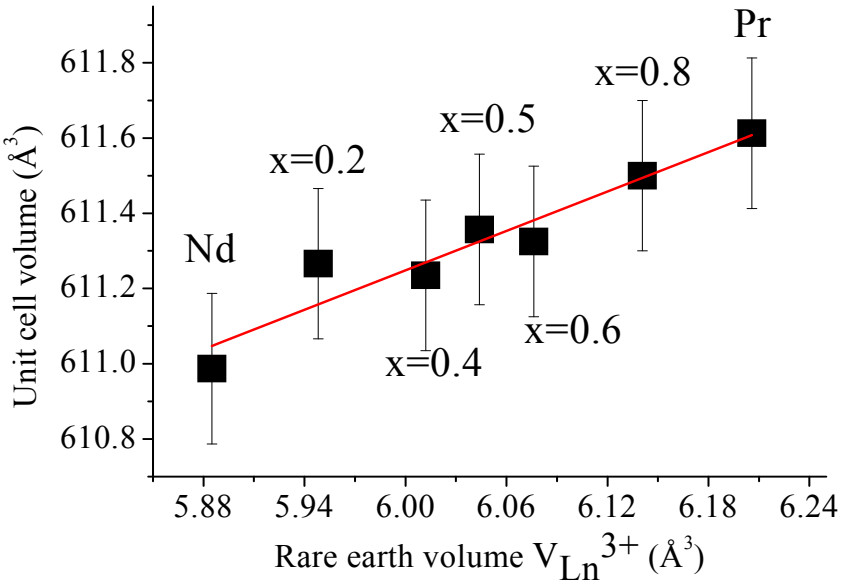
Pr
x=0.8
x=0.5
x=0.2
Nd
x=0.6
x=0.4
611.8
611.6
611.4
611.2
611.0
610.8
Unit cell volume (Å3)
5.88
5.94
6.00
6.06
6.12
6.18
6.24
Rare earth volume V Ln3+ (Å3)

Figure 3

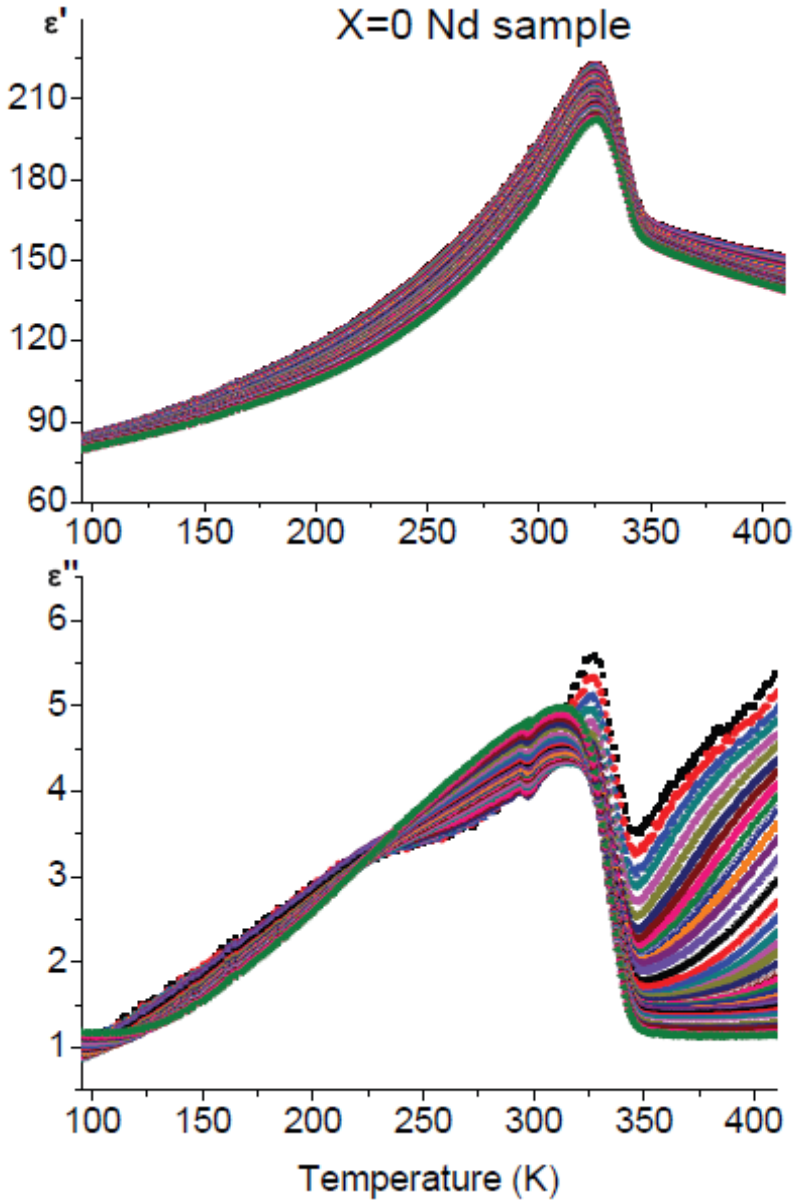
X=0 Nd sample
ε'
210
180
150
120
90
60
100
150
200
250
300
350
400
ε''
6
5
4
3
2
1
100
150
200
250
300
350
400
Temperature (K)

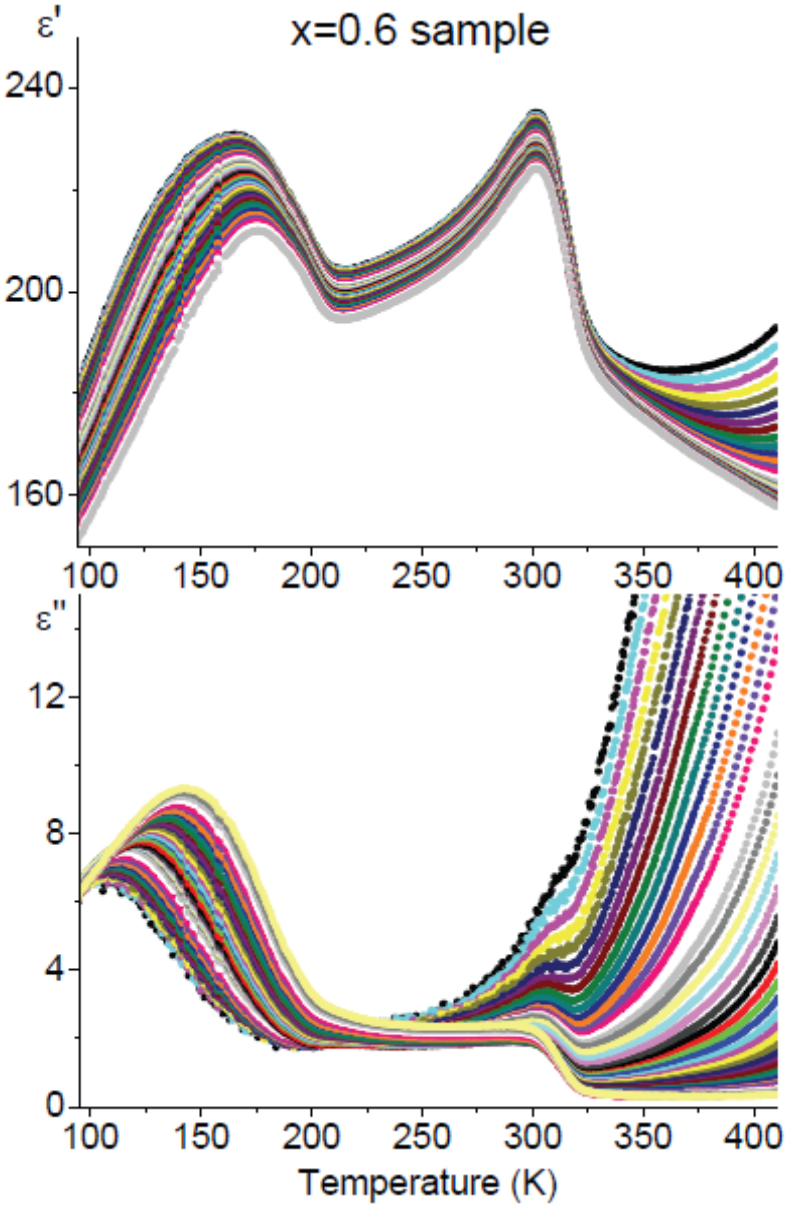
x=0.6 sample
ε'
240
200
160
100
150
200
250
300
350
400
ε''
12
8
4
0
100
150
200
250
300
350
400
Temperature (K)

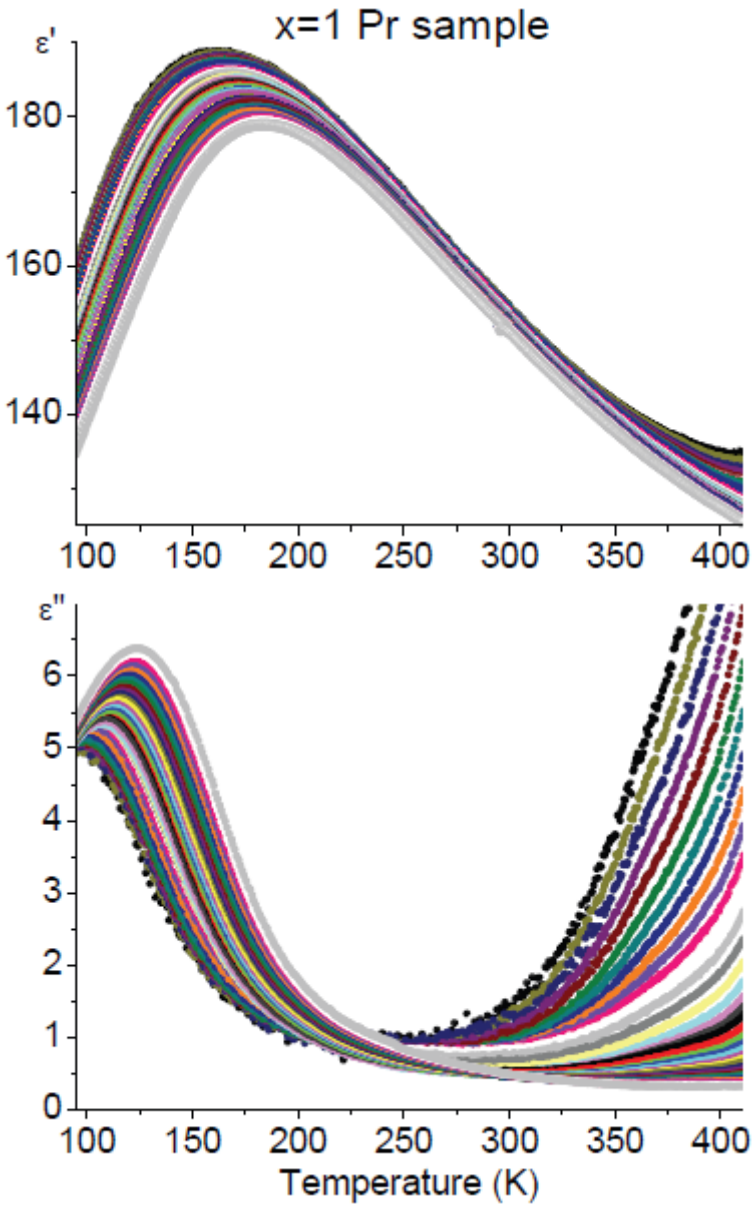
x=1 Pr sample
ε'
180
160
140
100
150
200
250
300
350
400
ε''
6
5
4
3
2
1
0
Temperature (K)

Figure 4

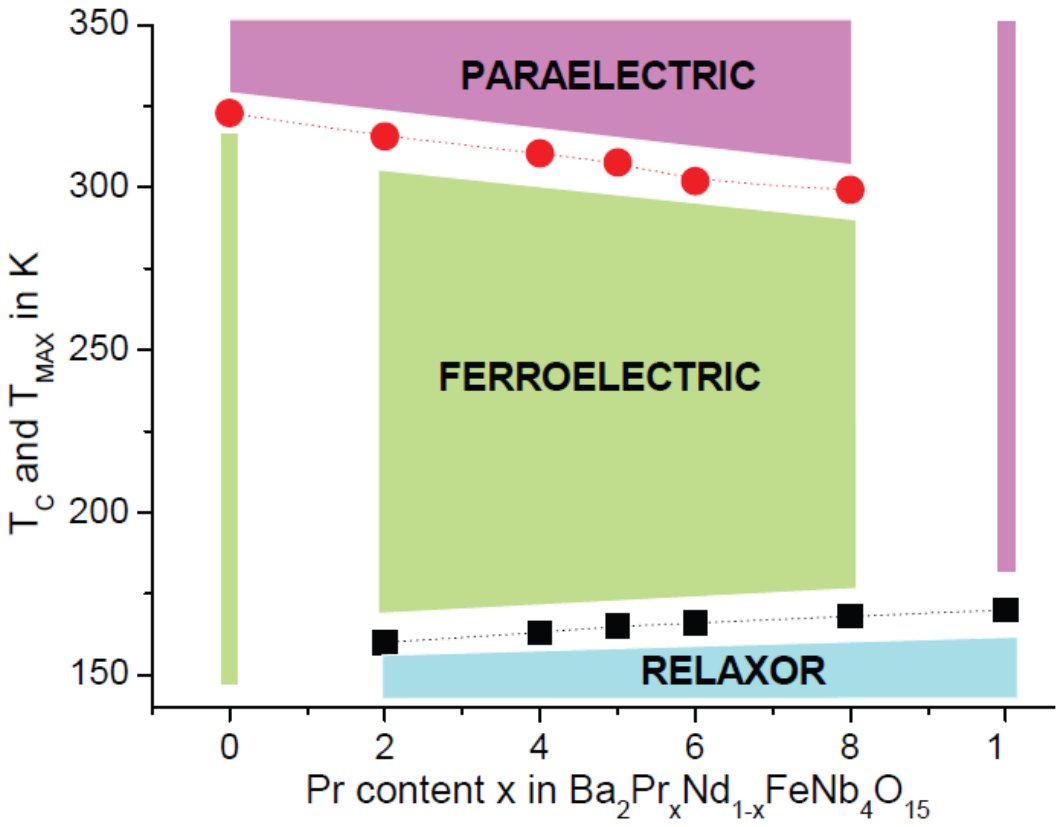
PARAELECTRIC
FERROELECTRIC
RELAXOR
350
300
250
200
150
0
2
4
6
8
1
T_C and T_MAX in K
Pr content x in Ba2PrxNd1-xFeNb4O15

Figure 5

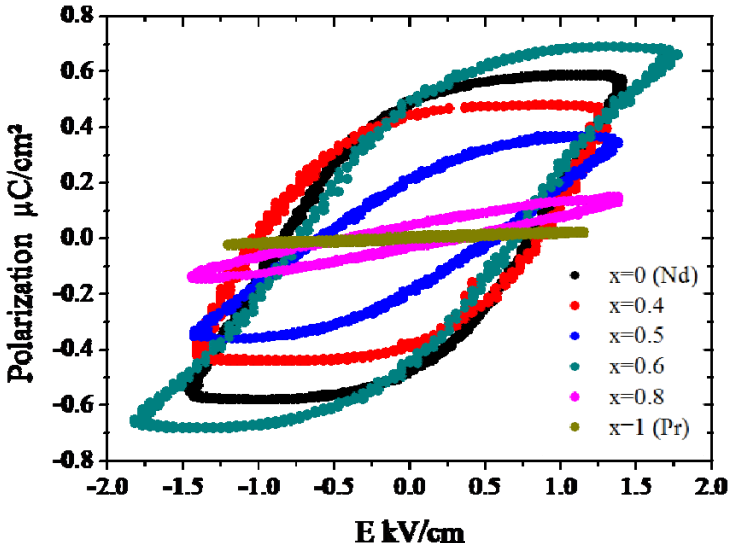

Figure 6

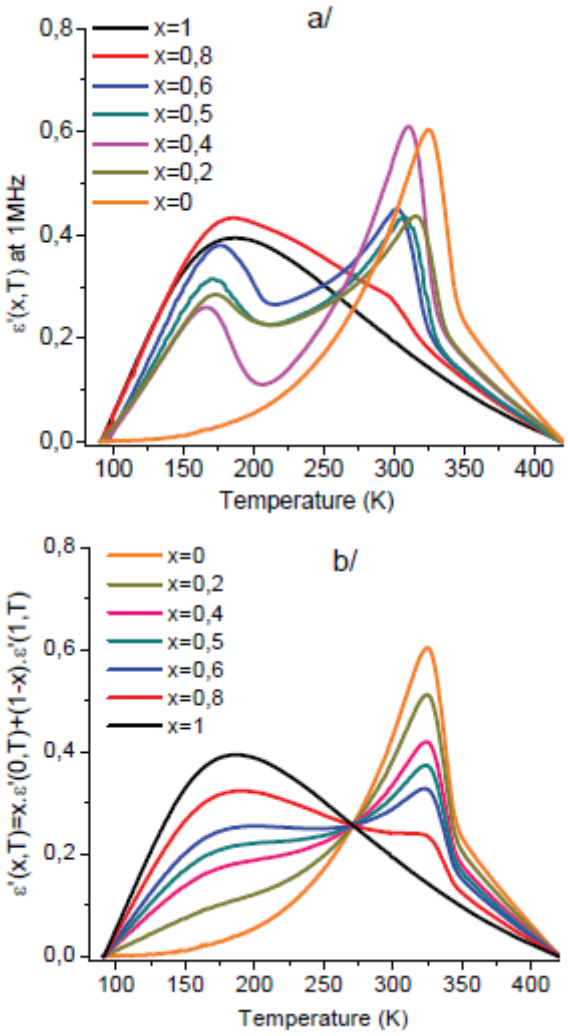
a/
x=1
x=0,8
x=0,6
x=0,5
x=0,4
x=0,2
x=0
ε'(x,T) at 1MHz
0,0
0,2
0,4
0,6
0,8
100
150
200
250
300
350
400
Temperature (K)
b/
x=0
x=0,2
x=0,4
x=0,5
x=0,6
x=0,8
x=1
ε'(x,T)=x.ε'(0,T)+(1-x).ε'(1,T)
0,0
0,2
0,4
0,6
0,8
100
150
200
250
300
350
400
Temperature (K)

Figure 7

Table caption 1: The activation energy E_A and the Vogel-Fulcher temperature T_{VF} versus Pr content x

x	T_{VF} (K)	E_A (eV)
0	--	--
0,2	152,36	0,03
0,4	149,76	0,024
0,5	149,29	0,031
0,6	141,91	0,053
0,8	128,57	0,089
1	110,16	0,121